April, 2005

Optimizing Vibration Isolation of Flex Circuits in Hard Disk Drives

M. R. Brake, *Carnegie Mellon University*
Jonathan A. Wickert, *Carnegie Mellon University*

Optimizing Vibration Isolation of Flex Circuits in Hard Disk Drives

M. R. Brake
Student Member

J. A. Wickert[1]
Fellow

e-mail: wickert@cmu.edu
Department of Mechanical Engineering, Data Storage Systems Center, Carnegie Mellon University, Pittsburgh, PA 15213

A "flex circuit" is a laminate of polyimide substrate, adhesive, and copper conductors that is used to connect the stationary electronic components in a computer hard disk drive to the rotating arm that positions read/write heads above the disks. The flex circuit's transverse and longitudinal vibrations couple with the arm, and those motions, although seemingly small, degrade performance during seek operations from one data track to another. The flex circuit and arm mechanism is defined by a number of geometric parameters, and some latitude is available at the design stage for choosing dimensions and angles so as to minimize vibration transmission from the flex circuit to the arm. In this paper, the results of parameter, optimization, and experimental studies are discussed with a view toward improving isolation of the arm from vibration of the flex circuit in one or several modes. Particularly for the mechanism's odd modes, the flex circuit's free length and the relative attachment angle between the arm's centerline and the circuit can each be chosen to significantly reduce vibration transmission. A genetic algorithm was applied to minimize a metric of vibration coupling in several vibration modes, and, in the case study examined, vibration isolation was improved by over 80%.
[DOI: 10.1115/1.1891813]

Introduction

Flex circuits are used to connect the stationary electronic and signal processing components in a computer's hard disk drive to the rotating arm that supports the read/write heads above the disks. In everyday use, the read/write heads are moved rapidly from one data track to another as files are created and accessed. Vibration of the flex circuit is unavoidably excited by such repositioning operations, and it couples with motion of the read/write heads across the width of the data tracks. Even seemingly small vibration of the read/write heads is undesirable because the data tracks are quite narrow. As data storage densities continue to grow, addressing and eliminating vibration sources that may previously have been within tolerance limits is one opportunity for improving the mechanical design of high performance disk drives.

Generally formed as a laminate of polyimide film, annealed copper wires, and epoxy adhesive, a flex circuit conveys all electrical signals between the (rotating) arm and read/write heads, and the (stationary) electronics block that is located on the drive's body. As indicated in the sketch of Fig. 1, the primary degrees of freedom available to a designer are the thicknesses of the individual layers within the circuit, the number of conductors and their placement relative to the flex circuit's width, the circuit's free length, and the locations and means of attachment between the flex circuit, the arm, and the electronics block. The extent of vibration transmission from the flex circuit to the arm further depends on the arm's rotation angle, which during usage varies randomly and nearly continuously between orientations at the disk's inner and outer diameters. In this paper, an existing model [1] for the natural frequencies and mode shapes of the flex circuit and arm is explored with a view toward optimizing geometry and the degree of vibration isolation.

The dynamics of the flex circuit and arm mechanism is a niche that falls within the broader context of vibration issues related to hard disk drives in computer data storage. Such components as the disks, spindle, bearings, suspension, arm, and voice coil actuator have already been the subject of substantial engineering and research efforts to reduce vibration and improve shock resistance. The vibration of the disks, spindle, and bearings is a key issue for applications involving high track density and rotation speeds. Hydrodynamic bearings in lieu of traditionally used ball bearings, alternative substrate materials that incorporate viscoelastic damping treatments, and tuned-mass dampers are three options that have been explored for reducing in-plane and out-of-plane disk vibration [2,3]. Shock response is particularly important in mobile computing applications, and the air bearing that forms between the slider's and disk's surfaces can be designed to reduce transient dynamic forces and damage to the read/write heads [4,5]. Airflow within the hard disk drive's enclosure, which is driven by rotation of the disks and spindle, can excite vibration and degrade positioning accuracy of the read/write heads. The arm partially obstructs this airflow, and the intensity of the vortices that form behind it, as well as the associated aerodynamically excited vibration, can be reduced by modifying the arm's geometry [6]. Constrained layer damping has also been investigated as a solution to reduce arm vibration and improve tracking dynamics. Such treatments have been attached to the housing of the arm's pivot assembly [7] and to the cover of the drive [8].

Aside from those topics, the present paper addresses vibration transmission between the flex circuit and arm, and the design implications. For each mode involving coupled longitudinal and transverse vibration of the flex circuit, and small amplitude rotation of the arm, a metric of vibration isolation is taken as the ratio of displacement at the read/write heads to that of the flex circuit. The results of parameter studies are discussed with respect to the arm's angle, the circuit's free length, the attachment angle between the arm and circuit, and the attachment angle of the circuit at the electronics block. Each case study captures trends as a single parameter is varied about a baseline design, and opportunities for better isolating the arm from flex circuit vibration are described. Configurations in which the vibration isolation metric is increased, reduced, or driven precisely to zero are identified, and qualitative differences in vibration transmission for the even and odd vibration modes are discussed. In practice, each of the mechanism's design parameters can be varied simultaneously over a range of realistic values, and, to that end, a genetic algorithm optimization method is applied to minimize vibration coupling between the flex circuit and arm. Beginning from a random population of arm and flex circuit configurations, each design was assigned a fitness or performance value based upon the extent of

[1]Corresponding author.

Contributed by the Technical Committee on Vibration and Sound for publication in the JOURNAL OF VIBRATION AND ACOUSTICS. Manuscript received May 30, 2003; final revision, June 3, 2004. Associate Editor: L. Bergman.

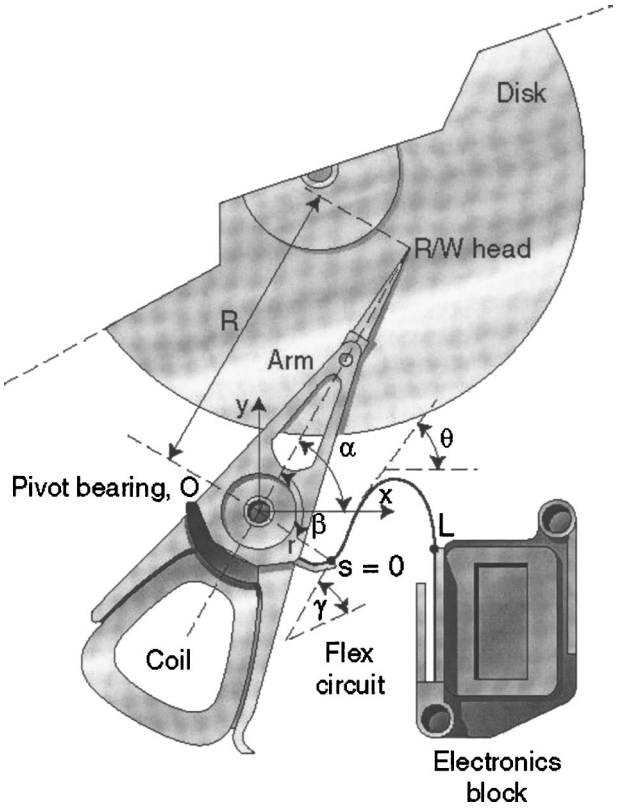

Fig. 1 Schematic of the vibration model for the arm and flex circuit mechanism in a hard disk drive

Table 1 Baseline parameters for the arm and flex circuit mechanism

Flex circuit	
Width, b	11.1 mm
Thickness	
Polyimide layer, h_p	31 μm
Adhesive layer, h_a	13 μm
Conductor layer, h_c	26 μm
Cumulative, h	114 μm
Conductor fraction, δ	67%
Free length, L	31 mm
Composite linear density, ρA	2.28 g/m
Modulus	
Polyimide, E_p	2.75 GPa
Adhesive, E_a	1.03 GPa
Conductor, E_c	115 GPa
Composite bending stiffness, EI	4.78×10^{-6} N·m^2
Composite axial stiffness, EA	2.45×10^{4} N
Arm	
Attachment radius, r	10.6 mm
Read/write head radius, R	43.8 mm
Attachment angle, β	95 deg
Offset angle. γ	8 deg
Inertia, m	17.2 g
Radius of gyration, κ	11.9 mm
Electronics block	
Coordinates, (X_L, Y_L)	(24, −11) mm
Tangency angle, θ_L	−90 deg

vibration isolation. In iteration, the population was bread and mutated within the context of natural selection principles so that the fittest designs would generally advance to the next generation. The results demonstrate that the mechanism can be designed successfully through this approach to significantly increase isolation of the arm from vibration of the flex circuit in certain modes, and in certain combinations of modes.

Arm and Flex Circuit Vibration Model

The vibration model for the flex circuit and arm involves four stages of deformation: the circuit's initial unstressed shape, configurations in which stresses set and relax in response to the disk drive's elevated temperature, equilibrium, and small amplitude vibration. Displacement of the flex circuit is resolved into the directions tangent and normal to the local equilibrium shape. In turn, those motions couple with the arm's dynamics. Nonlinearity associated with finite curvature, and the arm's geometry and inertia, are also incorporated within the model to predict natural frequencies, vibration modes, and the extent of circuit-to-arm coupling. This model is developed in [1], and reviewed here only briefly.

The flex circuit's shape is defined parametrically by the coordinates $(x(s,t),y(s,t))$ and slope $\theta(s,t)$, where s is the arc length coordinate and t denotes time. The circuit is subjected to internal tension T, shear N, and bending moment M. As shown in Fig. 1, the coordinates (x_L,y_L) of the contact point, and the angle θ_L of the circuit's approach, at the electronics block are specified at the right endpoint $s=L$. At the left endpoint $s=0$, the circuit has an initial slope with respect to the centerline of the arm. The deviation between the arm's axis and the tangent to the circuit at $s=0$ is termed the offset angle γ. The relative attachment angle β is defined as the angle between the arm's centerline and the circuit's point of attachment to the arm, measured about the pivot bearing point O. Rotation of the arm about its support point O is denoted by angle α, and together with the geometric parameters β, γ, and r defined in Fig. 1, its value sets the following boundary conditions at the circuit's left endpoint

$$x(0,t)=r\cos(\alpha-\beta),\quad y(0,t)=r\sin(\alpha-\beta),\quad \theta(0,t)=\alpha-\gamma \tag{1}$$

Through an external bias torque that is generated by the voice coil actuator shown in Fig. 1, the arm can be held at an equilibrium angle that corresponds to, for instance, the disk's inner (ID) or outer (OD) diameters, or any point between.

With the nomenclature $(\cdot)'=d/ds$, equilibrium in the flex circuit's tangential and normal directions is governed by the force and moment balances

$$T'=Nk,\quad N'=-Tk,\quad k'=-N/EI^{(2)\prime} \tag{2}$$

in which k denotes curvature in the deformed state, $k^{(2)}$ is the curvature in the flex circuit's natural state, and the Euler-Bernoulli constitutive relation $M=EI(k-k^{(2)})$ has been embedded. In terms of the quantities listed in Table 1 for the polyimide (p), adhesive (a), and conductor (c) layers of the circuit, its composite bending stiffness is

$$EI=\tfrac{1}{12}E_ch_c^3\delta b+\tfrac{1}{12}E_ah_c^3(1-\delta)b+2E_a\left(\tfrac{1}{12}bh_a^3+\tfrac{1}{4}bh_a(h_a+h_c)^2\right)+2E_p\left(\tfrac{1}{12}bh_p^3+\tfrac{1}{4}bh_p(2h_a+h_p+h_c)^2\right) \tag{3}$$

where δ is the fraction of the circuit's cross-sectional width b formed of conductor, and its axial stiffness is

$$EA=E_ch_cb\delta+2E_ah_ab+E_ah_cb(1-\delta)+2E_ph_pb \tag{4}$$

In each case, a symmetric cross section having one conductor layer that is sandwiched between adhesive and polyimide is specified. The circuit's equilibrium shape is found by direct integration of

$$x'=\cos\theta,\quad y'=\sin\theta,\quad \theta'=k(s) \tag{5}$$

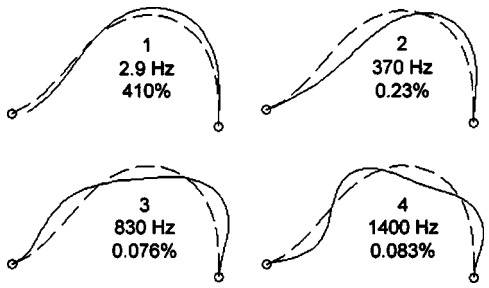

Fig. 2 First four vibration modes (—) shown superposed on the flex circuit's equilibrium shape (---). The mode shapes are annotated with the corresponding natural frequency and displacement ratio η.

The vibration model is linearized about equilibrium. The time-dependent and arc length-dependent corrections to the shear, tension, and curvature within the flex circuit are

$$N_1 = -EI(v_{,SS} + (k^* u)_{,S})_{,S} \tag{6}$$

$$T_1 = EA(u_{,S} - k^* v) \tag{7}$$

$$k_1 = (v_{,S} + (k^* u))_{,S} \tag{8}$$

in terms of the flex circuit's tangential u and normal v displacement components. Here the comma-subscript notation signifies partial differentiation, k^* denotes the equilibrium curvature, and quantities with the subscript "1" are first-order terms. The equations of motion for the flex circuit become

$$\rho A u_{,tt} - T_{1,S} + N^* k_1 + k^* N_1 = 0 \tag{9}$$

$$\rho A v_{,tt} - N_{1,S} - T^* k_1 - k^* T_1 = 0 \tag{10}$$

where ρA is the circuit's mass-per-unit-length, and quantities with an asterisk subscript are evaluated at their equilibrium values. Vibrations of the flex circuit and arm couple through

$$m\kappa^2 \ddot{\alpha}_1 = T_1(0,t) r \sin(\beta - \gamma) + N_1(0,t) r \cos(\beta - \gamma) + M_1(0,t) \tag{11}$$

where m is the arm's mass, κ is its radius of gyration about point O, and α_1 is the arm's first-order rotation about equilibrium.

The model is discretized through finite difference in order to obtain a matrix eigenvalue problem for the natural frequencies and mode shapes. The metric of vibration coupling between the flex circuit and arm is termed the modal displacement ratio and defined by

$$\eta = \frac{R|\alpha_1|}{\max(\sqrt{u^2 + v^2})} \tag{12}$$

Length R here and in Fig. 1 is the radius from the pivot point to the location of the read/write heads. This metric compares the relative motion between the read/write heads and the maximum vibration amplitude of the flex circuit in a given mode. That is, with η small, the motion of the read/write heads is a small fraction of the displacement present in the flex circuit. A design objective, therefore, may be to minimize η in certain modes or in certain combinations of modes. While other metrics can be chosen, in the following parameter and optimization studies, ratio (12) is taken as the metric of vibration coupling between the flex circuit and arm.

Figure 2 depicts the predicted equilibrium shape of the flex circuit and the mechanism's first four vibration modes for the baseline parameters of Table 1. The fundamental mode, which has a natural frequency of only 2.9 Hz, is associated with the sway of the arm in response to the flex circuit's (small) static stiffness. Because of its low natural frequency, the first mode is generally not of concern with respect to arm vibration following track-to-track seeks, and it is not considered further here. Of greater interest are the second, third, and higher modes that do involve significant elastic deformation of the flex circuit, and which can have natural frequencies beyond the bandwidth of the arm's servo control system (not shown in Fig. 1). Although the displacement ratios listed in Fig. 2 are only a fraction of a percent in modes 2–4, and seemingly small, they nevertheless have significant design implications because of the high positioning precision (on the order of ±25 nm for recording and ±50 nm for reading operations) that is required of this mechanism.

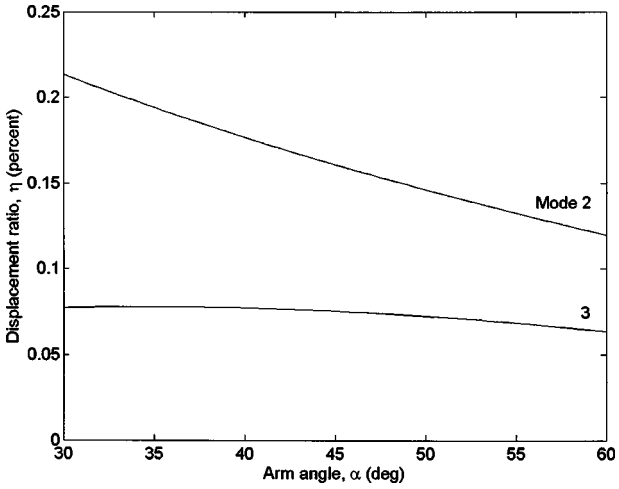

Fig. 3 Dependence of the displacement ratios for the second and third modes on the arm's position between the disk's inner (60 deg) and outer diameters (30 deg)

The manner in which the displacement ratios vary with position of the arm, and therefore with the point about which the model is linearized, is shown in Fig. 3. The odd vibration modes are generally less sensitive than the even ones to the arm's placement α on the disk between the ID (60 deg) and OD (30 deg). In the genetic-algorithm-based optimization study that follows, a weighted average of the displacement ratios evaluated at a number of points over the disk's surface is taken as the performance measure.

Mock Test Stand and Experiments

Figure 4 depicts the mock flex circuit and arm test stand that was used, in part, for model validation over a range of L, β, θ_L, γ, x_L, and y_L values. Stainless steel strip stock was used to mimic the flex circuit's elasticity, and the inertia of the arm was represented by a bearing, clamp, and rod assembly. The test stand was mounted on an optical bench so that the locations and angles of the connections to the strip's endpoints could be adjusted. The mock test stand is preferentially used for validation tests because its geometry can easily be varied, and related tests with actual disk drive hardware are described in [1].

Transverse vibration was measured by using a Michelson-style interferometer (Polytec OFV-502 and OFV-3000) that incorporates fiber optic leads to set paths for the reference and target laser beams. To ensure that sufficient light was returned into the optical head, a retroreflective coating was applied to the strip at each measurement point. Glass beads of diameter 40 μm within the retroreflective medium ensured that a portion of the incident light was returned into the source optical fiber even in the presence of misalignment between the laser head and strip, or in the presence of large deformations. With this technique, vibration measurements were readily made with a strong signal-to-noise ratio and with resolution and bandwidth exceeding the requirements for model validation.

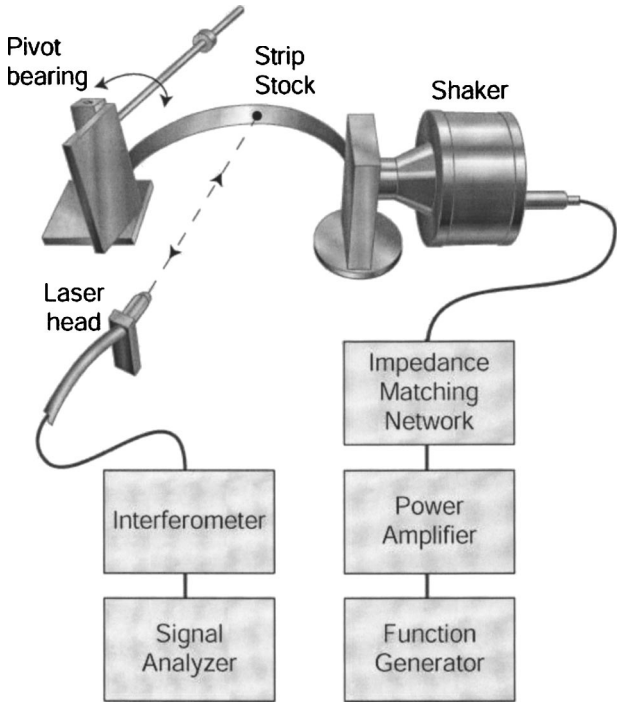

Fig. 4 Illustration of the mock arm and flex circuit test stand

Vibration was measured as the mock arm and flex circuit assembly was excited by a voice coil shaker driven through a matching network by a power amplifier (Wilcoxon Instruments F-4, PA-7D, and N-7C). The shaker was attached to the "arm electronics" support at $s=L$ and driven near a natural frequency. In the steady state, the displacement components of the strip (in the directions normal and tangent to equilibrium) were measured at multiple positions along its length in order to capture the in-plane mode shapes. While the normal motion could have been measured in a noncontact manner through alternative means (for instance, an eddy current sensor), it is more problematic to measure the strip's tangential motion. The normal and tangential motions were measured for the second, third, and fourth modes by exploiting the characteristics of the retroreflective coating that was applied to the strip's surface. With the interferometer's laser beam directed perpendicular to the strip, the normal displacement component v was measured, as is conventional. Subsequently, with the beam oriented at an oblique angle (generally 45 deg) relative to normal, a superposition of the strip's normal and tangential motions was recorded. By capturing time records of the strip's motion in two linearly independent directions, and by appropriately reducing such measurements, both u and v were obtained in a noncontact manner.

Experiments were conducted to verify the natural frequencies, mode shapes, and displacement ratios (12) that are predicted by the vibration model. For the test stand parameters listed in Table 2, Figs. 5–7 compare the measured and predicted u-v mode shapes for the second, third, and fourth vibration modes. Likewise, Fig. 8 compares the measured and predicted metrics η for those modes. Correlation of the results is generally satisfactory.

Case Studies in the Design Parameters

Several parameter studies were conducted in the following design variables, as identified in Fig. 1 and with nominal values listed in Table 1:

1. the flex circuit's free length L,

Table 2 Parameters for the mock arm and flex circuit test stand

Width, b	25.4 mm
Thickness, h	203 μm
Free length, L	34.9 cm
Density, ρ	7750 kg/m^3
Modulus, E	210 GPa
Springback ratio, p	0.93
Attachment radius to arm, r	49 mm
Arm radius, R	457 mm
Relative attachment angle, β	80 deg
Offset angle, γ	7 deg
Arm assembly inertia, m	1.03 kg
Radius of gyration, κ	22 cm
Endpoint coordinates, (X_L, Y_L)	(28, −1.6) cm
Endpoint tangency angle, θ_L	−90 deg

2. the relative attachment angle β between the arm's centerline and the flex circuit's left end $s=0$ and point of attachment to the arm,
3. the tangency angle θ_L at which the flex circuit approaches the stationary arm electronics block, and

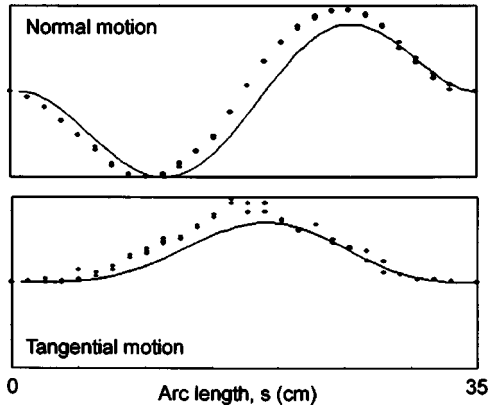

Fig. 5 Comparison of measured (···) and predicted (—) second mode shapes. The normal and tangential components are shown on the same scale. Multiple points indicate separate trials.

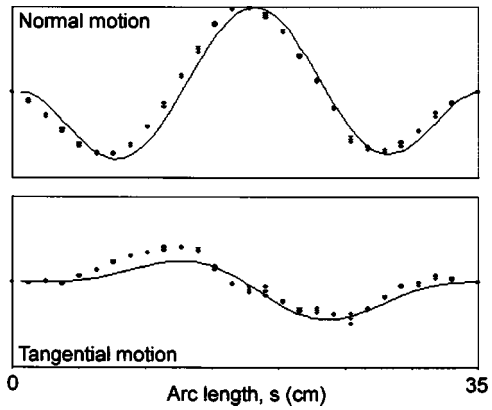

Fig. 6 Comparison of measured (···) and predicted (—) third mode shapes. The normal and tangential components are shown on the same scale. Multiple points indicate separate trials.

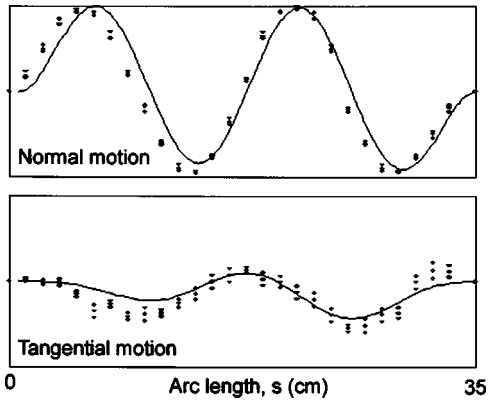

Fig. 7 Comparison of measured (···) and predicted (—) fourth mode shapes. The normal and tangential components are shown on the same scale. Multiple points indicate separate trials.

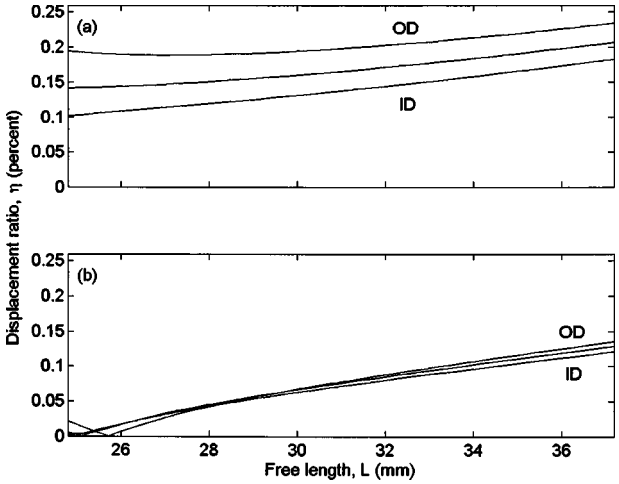

Fig. 9 Dependence of the (*a*) second and (*b*) third mode displacement ratios on the flex circuit's free length, for arm positions at the disk's inner (ID), middle, and outer (OD) diameters

4. the offset angle γ which sets the slope of the flex circuit at $s=0$ relative to the arm's centerline.

In each case, one design variable was adjusted around its baseline value, with the other parameters being held constant. To the extent that the arm sweeps across the disk's surface during operation, the equilibrium value of α was set to the inner, middle, and outer disk positions to assess the sensitivity of η to the arm's position. As borne out in Figs. 9 and 12–14, the odd modes are relatively insensitive to the arm's equilibrium position. For the even modes, the displacement ratios are generally lower at the ID than at the OD by some 20%–50%.

The discussion of metric η is limited to the second and third modes, which primarily contribute to the arm's transient motion, and which have behavior qualitatively similar to that of the higher even and odd modes, respectively. Figure 9 depicts variation of the displacement ratios for modes two and three with respect to the flex circuit's free length. In the second mode (Fig. 9(*a*)), η is relatively insensitive to changes in L about the nominal value of Table 1, and it increases by only a modest amount as the arm slews between the disk's ID and OD. On the other hand, in Fig. 9(*b*), η for the third mode has a zero crossing near 26 mm, and the zero crossing is relatively insensitive to the arm's position. The modal displacement ratio evidently can be reduced significantly, and in principle driven to zero, by optimal selection of the free length to a value some 83% of its baseline value. The fifth vibration mode also has a zero crossing at essentially the same value of L.

For the purpose of model validation, measurements in L were conducted with the mock flex circuit test stand. The third mode's measured and predicted natural frequencies and displacement ratios are compared in Figs. 10 and 11. This mode was selected in order to validate the existence of a geometric configuration in which the third mode would have little contribution to dynamic coupling between the flex circuit and the arm. In the experiments, the natural frequency decreased with L, and the coupling metric had a zero crossing near the value 31 cm. The root-mean-square difference between the measured and predicted η values is 6×10^{-5}.

Like free length, the relative angle β between the arm's centerline and the circuit's attachment point $s=0$ can have a significant effect on vibration coupling between the flex circuit and arm. Figure 12 depicts the dependence of the displacement ratios in the second and third modes, and both η_2 and η_3 decrease as β is increased above its nominal value. Near $\beta=110$ deg, in fact, the ratio for the third mode has a zero crossing, and the ratio for mode 2 has even been lowered by some 40% relative to the baseline

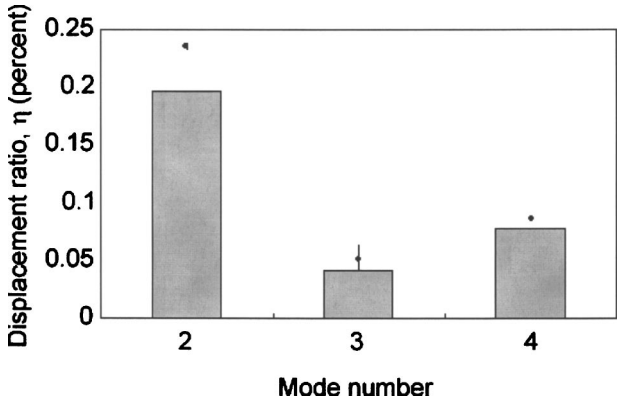

Fig. 8 Predicted (bars) and measured (points) displacement ratios for the mock flex circuit test stand in the second, third, and fourth vibration modes. The measured values are averages of three independent trials. Data ranges are indicated by the narrow bars through each point.

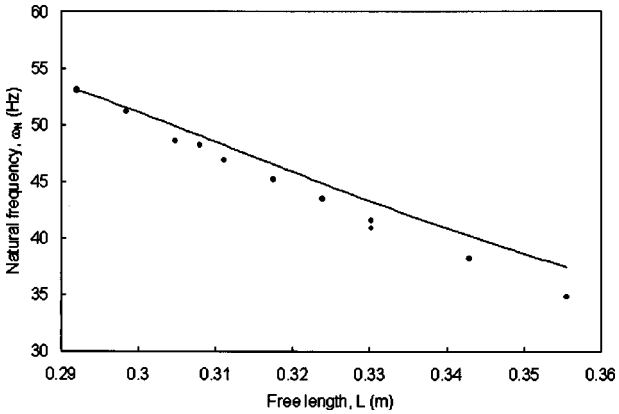

Fig. 10 Comparison of measured (···) and predicted (—) natural frequencies of the mock arm and flex circuit test stand in the third vibration mode. Multiple points indicate separate trials.

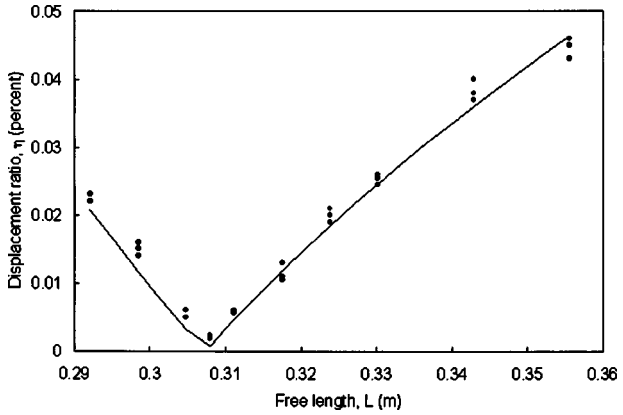

Fig. 11 Comparison of measured (···) and predicted (—) displacement ratios of the mock arm and flex circuit test stand in the third vibration mode. Multiple points indicate separate trials.

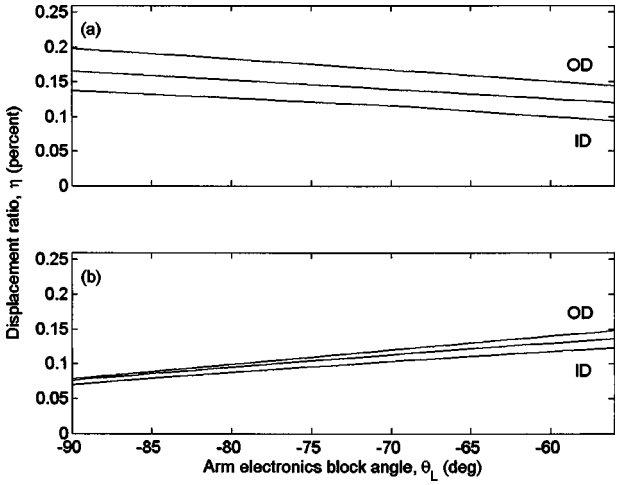

Fig. 13 Dependence of the (*a*) second and (*b*) third mode displacement ratios on the orientation angle of the arm electronics block, for arm positions at the disk's inner (ID), middle, and outer (OD) diameters

design. For applications in which vibration of the third mode is problematic, that value of the attachment angle could be selected as optimal.

Figures 13 and 14 depict the results of parameter studies in the angle θ_L at which the flex circuit approaches the stationary electronics block, and in the tangency angle γ of the flex circuit relative to the arm's centerline. In each case, the displacement ratios are larger with the arm set at the disk's OD than at the ID. For θ_L and γ, the ratio in the third mode grows monotonically as the angles are independently increased. For the second mode, the metric increases with γ but decreases slightly with θ_L. In the next section, potential interactions among the design variables and the trends indicated by Figs. 9 and 12–14 are investigated further from the standpoint of multi-parameter optimization.

Optimization Through a Genetic Algorithm

A genetic algorithm is a search-based optimization method in which an ensemble or population of trial solutions is adjusted in structured iteration. A "survival of the fittest" strategy is employed based on the principles of natural selection. In terms of a performance function (for instance, the displacement ratio for a particular mode, or a weighted average of η for a group of modes), the fittest members of the population reproduce and pass their performance attributes forward to the next generation. Genetic algorithms are typically able to pursue several promising solutions simultaneously in order to explore or cover a wide range of the potential solution space. Likewise, poor designs (namely, ones having large displacement ratios in certain critical modes) generally will not persist and effectively reproduce, except by intentional chance which is allowed.

The search method is initialized with a randomly constructed population of arm and flex circuit mechanism designs. Designs are selected and then updated through two processes termed mutation and cross-over. In mutation, the characteristics of a design are randomly altered and passed to the next generation. On the other hand, cross-over combines two designs in terms of their "chromosome" vectors comprising the design parameters in order to yield two new designs. A probabilistic method based on the degree of fitness is employed to select those designs that reproduce and seed subsequent generations [9,10].

The optimal selection of geometric parameters can be a useful technique for passively controlling vibration. However, complicated nonlinear relationships can exist between the design parameters and the cost function being used in optimization, and the

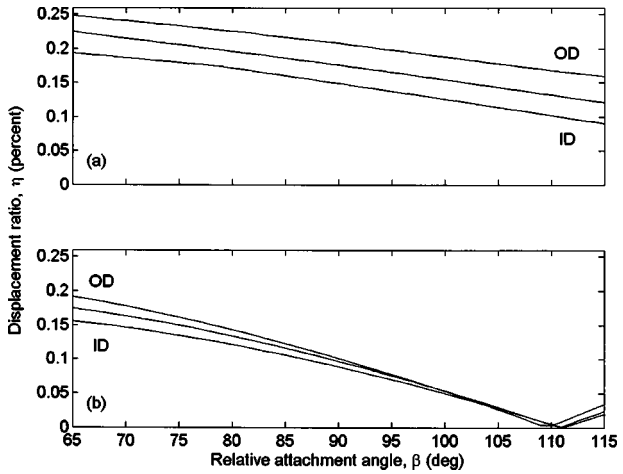

Fig. 12 Dependence of the (*a*) second and (*b*) third mode displacement ratios on the relative attachment angle between the flex circuit and arm, for arm positions at the disk's inner (ID), middle, and outer (OD) diameters.

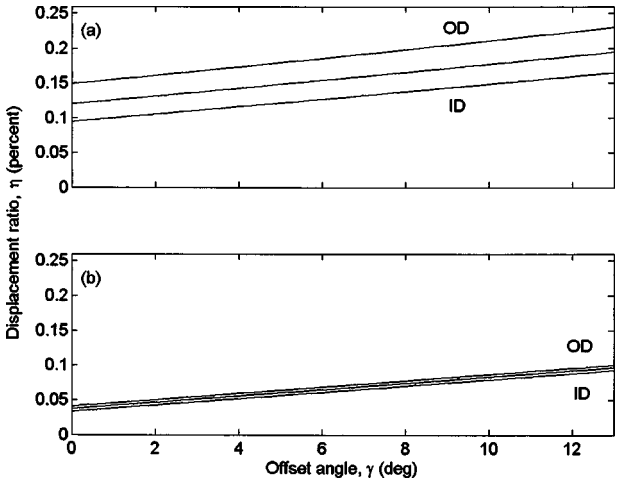

Fig. 14 Dependence of the (a) second and (b) third mode displacement ratios on the offset angle between the flex circuit and arm, for arm positions at the disk's inner (ID), middle, and outer (OD) diameters

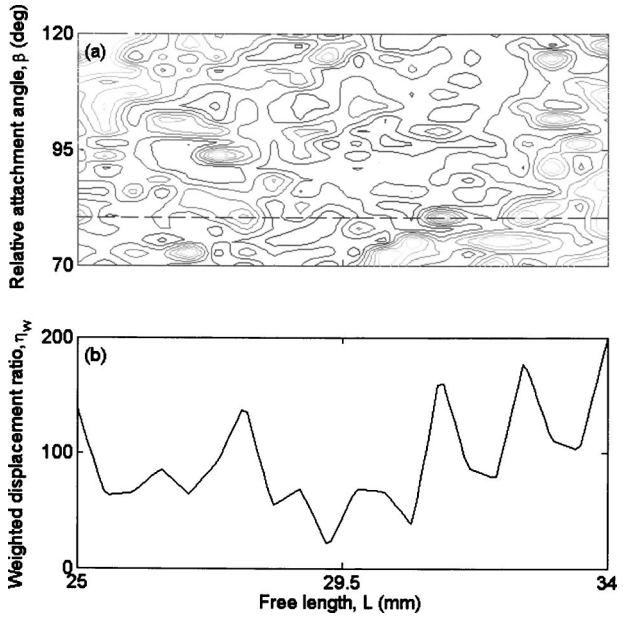

Fig. 15 (a) Cross section of the weighted displacement ratio's surface along the plane L-β in the design space, indicating the presence of multiple local minima. (b) Cross-section of the weighted displacement ratio along L for β=80°.

topology of the cost function can encompass multiple local minima. Particularly when each configuration is expensive to evaluate, traditional gradient-based search methods can experience numerical difficulties, but genetic algorithms can be more robust, outperforming other evolutionary-based techniques. The geometry of a two-dimensional truss structure, for instance, has been successfully optimized by this approach with respect to energy flow over a range of frequencies [11–13].

The performance measure for the arm and flex circuit mechanism was chosen as the root-mean-square sum of the displacement ratios η in the second, third, and fourth vibration modes. In order to capture variation that occurs as the arm sweeps across the disk, this so-called weighted ratio η_w was taken as the average of evaluations at seven arm positions α recorded every 5 deg between the disk's OD and ID. The ratio was further normalized so that the baseline design rated a fitness level of 100%. The objective of evolution from one generation to the next was to minimize η_w over realistic bounds of the geometric design parameters.

The rationale behind using a genetic algorithm recognizes the computational expense associated with evaluation of each design, and the presence of many local minima in which gradient-based search methods can become trapped. The mechanism's design space comprises the six parameters $(L, \beta, \theta_L, \gamma, x_L, y_L)$. An exhaustive search over all variables is not computationally feasible. In a cross-section of the design space along only the plane defined by the free length L and the relative attachment angle β, over 50 local minima exist. Figure 15 depicts the complicated topology of the weighted displacement ratio as a function of L and β. Along higher-dimensional sections of the design space, the cost function is expected to have even more detailed behavior, challenging the use of gradient-based methods.

An initial population of 50 arm and flex circuit mechanisms was created having normally distributed values of $(L, \beta, \theta_L, \gamma, x_L, y_L)$ centered around the nominal values listed in Table 1, with all other parameters remaining fixed. Figure 16 summarizes the manner in which the optimization progressed through 80 generations. Most improvement occurred early in the iteration cycle, specifically within the first five generations. The weighted displacement ratio of the final "optimal" solution was 82% lower

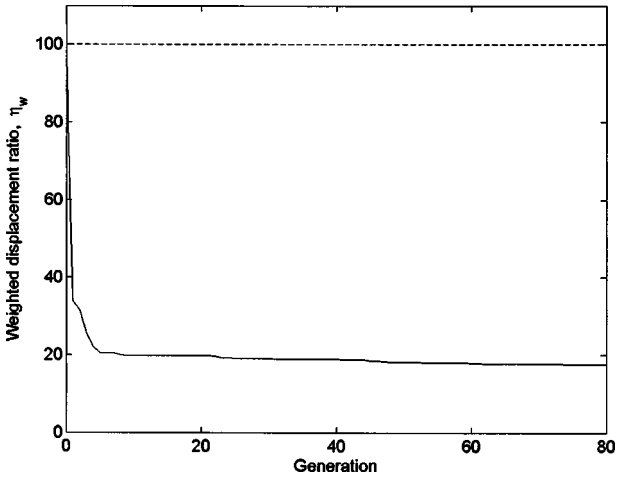

Fig. 16 Progress of the genetic algorithm toward the optimal (—) solution with each successive generation compared to the baseline solution (---)

than that of the baseline design. Viewed from another standpoint, the baseline design presents over five times more transmission of vibration from the flex circuit to the arm in the second, third, and fourth modes, as averaged over the disk's surface. Table 3 lists the baseline and optimal parameter values, and illustrates the equilibrium shape of the flex circuit in the two configurations. Figure 17 depicts the improvement of the displacement ratios for the optimal solution in the second, third, and fourth modes, as compared to the baseline design. While the arm can be isolated from vibration in the flex circuit's odd modes by judicious selection of either L or β, as indicated in Figs. 9 and 12, isolation of the even modes is more problematic but achievable in the present case by exploiting interactions among the six design parameters.

Summary

The free length of a flex circuit, and the locations and angles of its attachment points to the arm and electronics block in a hard disk drive, can be selected preferentially in order to significantly

Table 3 Parameter values for the baseline and optimized flex circuit-arm geometries

Model parameter	Baseline	Optimized
Free length, L	31 mm	29.4 mm
Tangency angle, θ_L	-90 deg	-67.8 deg
Relative attachment angle, β	95 deg	118 deg
Offset angle, γ	8 deg	2.22 deg
Endpoint position, x_L	24 mm	21.0 mm
Endpoint position, y_L	-11 mm	-8.85 mm
Weighted displacement ratio, η_w	100%	17.7%
Equilibrium shape		

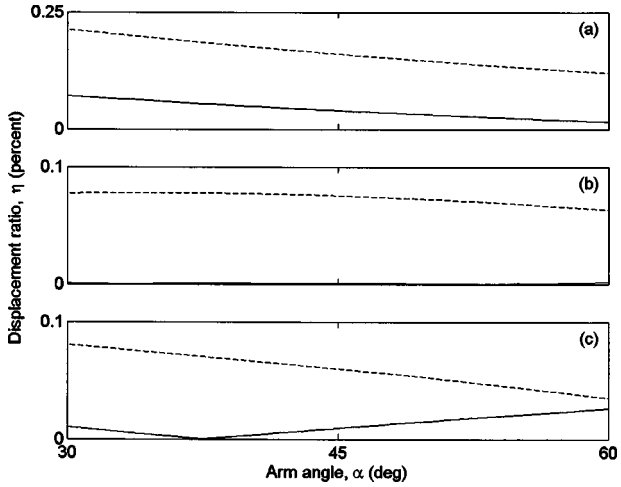

Fig. 17 Comparison of the displacement ratios of the baseline (---) and optimized (—) flex circuit shapes on the arm's position between the disk's inner (60 deg) and outer diameters (30 deg) for the second (*a*), third (*b*), and fourth (*c*) modes

decrease the transmission of vibration from the flex circuit to the arm. In parameter and optimization studies of the variables $(L, \beta, \theta_L, \gamma, x_L, y_L)$, the mechanism's design space was explored with a view toward reducing arm-circuit coupling in certain vibration modes, and in certain combinations of modes. Particularly for the odd modes, the flex circuit's free length L and the relative attachment angle β can each have a significant role in reducing vibration coupling between the flex circuit and arm. Specifically, zero crossings of the displacement ratios exist for the odd modes. A genetic algorithm, which is a structured search-based optimization method, was applied to minimize the root-mean-square displacement ratio over the second, third, and fourth vibration modes. The method was successful in improving vibration isolation by some 82%, which is viewed as a potentially useful improvement for the technology at hand.

Acknowledgments

This work was supported by a grant from IBM Corporation and Hitachi Global Storage Technologies. The authors gratefully acknowledge use of the Genetic Algorithm Optimization Toolbox developed by C. Houck, J. Joines, and M. Kay of North Carolina State University.

References

[1] Wickert, J. A., 2003, "Free Vibration of Flex Circuits in Hard Disk Drives," ASME J. Vibr. Acoust., **125**(3), pp. 335–342.
[2] Shen, I. Y., 2000, "Recent Vibration Issues in Computer Hard Disk Drives," J. Magn. Magn. Mater., **209**, pp. 6–9.
[3] Bittner, H., and Shen, I. Y., 1999, "Taming Disk/Spindle Vibrations Through Aerodynamic Bearings and Acoustically Tuned-Mass Dampers," IEEE Trans. Magn., **35**(2), pp. 827–832.
[4] Jayson, E. M., Murphy, J., Smith, P. W., and Talke, F. E., 2003, "Effects of Air Bearing Stiffness on a Hard Disk Drive Subject to Shock and Vibration," ASME J. Tribol., **125**, pp. 343–349.
[5] Lin, C.-C., 2002, "Finite Element Analysis of a Computer Hard Disk Drive Under Shock," ASME J. Mech. Des., **124**, pp. 121–125.
[6] Kubotera, H., Tsuda, N., Tatewaki, M., and Maruyama, T., 2002, "Aerodynamic Vibration Mechanism of HDD Arms Predicted by Unsteady Numerical Simulations," IEEE Trans. Magn., **38**(5), pp. 2201–2203.
[7] Gao, P., Xu, L., Lin, R., and Tan, H., 2001, "Effect of the Pivot Assembly on the Dynamic Behaviour of a Head Actuator in Hard Disk Drives," Proc. Inst. Mech. Eng., Part C: J. Mech. Eng. Sci., **215**(4), pp. 461–467.
[8] Jiang, L., and Miles, R. N., 1999, "A Passive Damper for the Vibration Modes of the Head Actuator in Hard Disk Drives," J. Sound Vib., **220**(4), pp. 683–694.
[9] Goldberg, D., 1989, *Genetic Algorithms in Search, Optimization, and Machine Learning*, Addison-Wesley, Reading, MA.
[10] Houck, C. R., Joines, J. A., and Kay, M. G., 1996, "Comparison of Genetic Algorithms, Random Restart, and Two-Opt Switching for Solving Large Location-Allocation Problems," Comput. Oper. Res., **23**(6), pp. 587–596.
[11] Keane, A. J., 1995, "Passive Vibration Control Via Unusual Geometries: The Application of Genetic Algorithm Optimization to Structural Design," J. Sound Vib., **185**(3), pp. 441–453.
[12] Anthony, D. K., Elliott, S. J., and Keane, A. J., 1999, "Robustness of Optimal Design Solutions to Reduce Vibration Transmission in a Lightweight 2-D Structure, Part I: Geometric Design," J. Sound Vib., **229**(3), pp. 505–528.
[13] Anthony, D. K., and Elliott, S. J., 2001, "On Reducing Vibration Transmission in a Two-Dimensional Cantilever Truss Structure Using Geometric Optimization and Active Vibration Control Techniques," J. Acoust. Soc. Am., **110**(2), pp. 1191–1194.